CHRISTOF SCHÜTTE, ANDREAS HOHMANN AND MANFRED DINAND

Numerical Simulation of Relaxation Oscillations of Waveguide-Lasers

NUMERICAL SIMULATION OF RELAXATIONS OSCILLATIONS OF WAVEGUIDE-LASERS

CHRISTOF SCHÜTTE[+], ANDREAS HOHMANN[+], AND MANFRED DINAND[*]

([+]) KONRAD–ZUSE–ZENTRUM BERLIN
HEILBRONNER STR. 10, D-10711 BERLIN, GERMANY
SCHUETTE@SC.ZIB-BERLIN.DE

([*]) ANGEWANDTE PHYSIK, UNIVERSITÄT-GH-PADERBORN,
WARBURGER STR. 100, D-33098 PADERBORN, GERMANY

Abstract. An analysis of relaxation oscillations in local Er-doped optically pumped waveguide lasers is reported. It is based on a time dependent rate equation model for a quasi-two-level-system with wavelength dependent emission- and absorption cross-sections. For the first time a numerically reliable simulation of the characteristic laser behaviour was possible: the onset and decay of the oscillations, the time-dependent repetition period and the steady state signal output power. The characteristic waveguide parameters, as the erbium-concentration profile, the polarization dependent pump- and signal mode intensity profiles, the scattering losses, the cavity length and the front and rear reflectivities were all taken into account. The basic formulas are general and can also be used for Er-doped fiber lasers. Mathematically the problem can be characterized as a large boundary value problem, which can approximately be replaced by a stiff initial value problem of ordinary differential equations. The used algorithmic replacement procedure is motivated and discussed in detail.

Here, pump- and signal evolution versus time are presented for an planar Er-diffused Ti:LiNbO$_3$ waveguide laser. The numerically obtained results show a nearly quantitative agreement with experimental investigations. Simultanously they supply knowledge about non–measureable (space–dependent population dynamic of the Er–atoms) and till today not measured data (dynamical response of the laser by a sharp peak in the external pump).

Key Words. relaxation oscillations, waveguide lasers, occupation dynamics,

Contents. 1 Introduction

1. Introduction. One of the most notable transient effect in solid-state lasers is the phenomenon of *relaxation oscillations* (a sequence of fairly sharp pulses in the output signal which ends in a steady state of constant laser output, see Fig. 1). On the one hand, in many laser applications it can be a problem, because fluctuations in the signal output are often unwanted. On the other hand it is an important tool to investigate basic laser parameters: relaxation oscillations take place with a characteristic period, which is much longer than the cavity decay time or the resonator roundtrip time and a well defined damping decay time. The physical mechanism is an interplay between the pump- and signal intensities within the resonator and the atomic inversion.
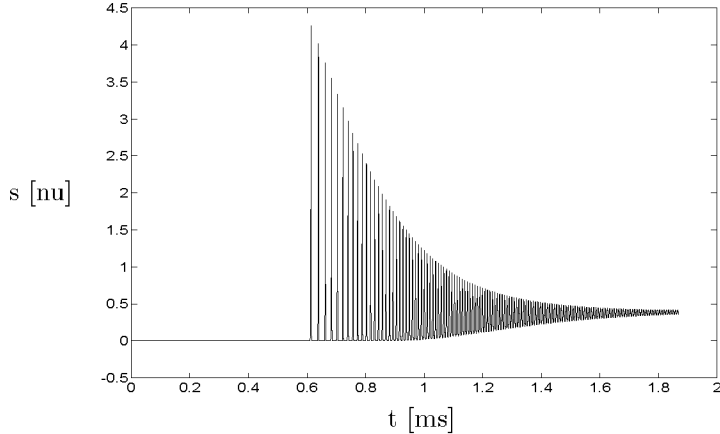

FIG. 1. *Relaxation oscillations of an erbium-diffused Ti:LiNbO₃ waveguide laser: signal output power s (in normalized units; see section 4) in forward direction versus time*

In this paper, we present an accurate analysis of relaxation oscillations in local Er-doped optically pumped waveguide structures. We have based our model on the time-dependent quasi-two-level-laser rate equations and on the equation of continuity for a gain medium. The local doped erbium concentration and the pump- and signal mode intensity profiles are taken into account as well as the front and rear refectivites of the Fabry-Perot-cavity, the scattering losses and the length of the cavity. The resulting system of partial differential equations for the intensities couples with an ordinary differential equation for the inversion; together they form a boundary value problem (BVP). We present an algorithmic procedure to replace this BVP by an initial value problem (IVP) of ordinary differential equations only. It will be shown, that the solution of this IVP is an excellent approximation of the solution of our model-BVP and that — fortunately — it is much easier to solve by numerical means.

The derived formulae are general and can be used for studying relaxation oscillations in different kinds of dielectric waveguide lasers. Different doping techniques, as for example Er-indiffusion or Er-implantation, which result in different Er-concentration profiles can be investigated as well as different fabrication methods of optical waveguides like indiffusion or proton exchange.

Herein, we particularly study simulation calculations of relaxation oscillations in *Er-diffused Ti-diffused LiNbO₃* dielectric waveguide lasers (with signal wavelength range around $\lambda_s \approx 1.5\mu m$ and pump wavelength $\lambda_p \approx 1.48\mu m$). The development of this class of lasers promise new applications in optical communications. Up to now, cw-laser operation has been obtained at four different wavelengths (1532 [1], 1563, 1576 nm [2] and 1602 nm [3]). In combination with other passive devices advanced integrated optical devices should be realizable in this material

1

system.

In section 2 and 3 the theoretical model is presented. The discussion of the basic evolution equations in section 2 results in the named boundary value problem. In section 3 the replacement procedure (BVP → adequate IVP) is motivated and constructed and in section 4 some comments on the used numerical methods are given. In the following paragraph (section 5) the numerically calculated results are presented and compared with experimental investigations. This paper will close with some results from simulation calculations, which show the possibilities of the herein demonstrated method by applying it to a situation which has not been realized experimentally till today.

2. Derivation of a Boundary Value Model. The solid state lasers we are interested in consist of an Er-doped waveguide which is limited by two dielectric mirrors vertical to the propagation direction. The optical channel of the waveguide is included in the region of main Er–dopant concentration as it can be seen schematically in Fig. 2.
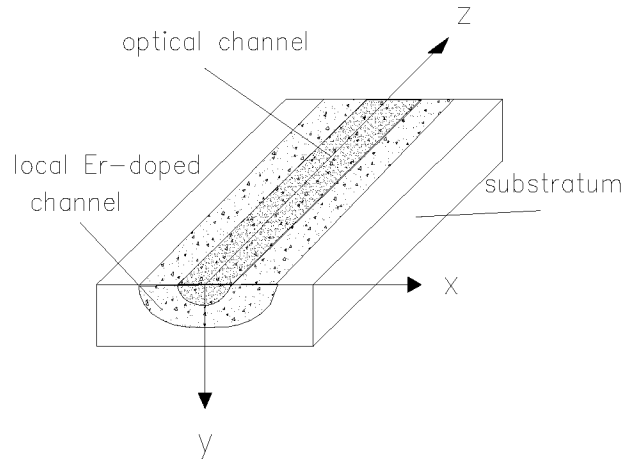

FIG. 2. *Local Er-doped optical channel waveguide*

In this region the concentration of Er^{3+}–ions is not uniform, but has got a particular space–dependency $N_0(x, y)$, which results from the indiffusion process of the Er^{3+}–ions starting at the x, z–plane. By analogy the intensity profile $I(x, y, z, \lambda, t)$ of the guided light (with wavelength λ) is space–dependent. A characteristical normalized intensity distribution $i_0(x, y, \lambda)$ belongs to each guided light wavelength ("mode" λ); it depends on the geometrical details of the waveguide.

The light matter interaction causing amplification (and/or laser effects) in these materials is that between the guided light and the Er^{3+}–ions: The *pump mode* (with wavelength λ_p, which is coupled into the waveguide from an external source) populates an excited state of the Er^{3+}–ions at the cost of their ground state. The effected *signal mode* (with a specific wavelength λ_s, which depends on the two involved levels of the Er^{3+}–ions) depopulates it. In order to build a model for the description of these effects we have to model

- the level structure of the dopant–atoms together with the transient behaviour of the level's population,

2

- the motion of the guided modes through the locally doped waveguide along the propagation direction z,
- the interaction between the intensity distribution and the population distribution in dependency from space and time.

Level populations. As a model to describe optical amplification by stimulated emission in Er–doped waveguides in the wavelength range around $1.55\,\mu$m, optically pumped at $\lambda_p \approx 1.48\,\mu$m, the quasi-two-level system, as shown in Fig. 3, can be used. Hence we simply speak of *the* ground and *the* excited state of the Er^{3+}–ions. Excited State Absorption (ESA) and Amplified Spontaneous Emission (ASE) have been neglected [5].
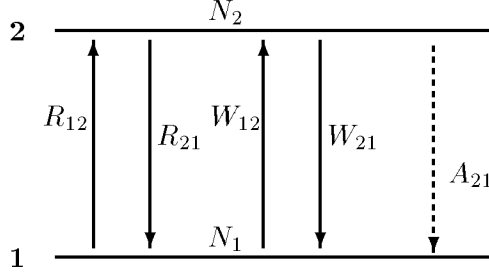

FIG. 3. *Quasi-two-level-model with pump (signal) absorption and emission rates R_{12} (W_{12}) and R_{21} (W_{21}), respectively. A_{21} is the spontaneous transition rate.*

The energy fine structure due to the Stark-effect can be taken into account by wavelength dependent absorption and emission cross-sections. The pump (signal) absorption and emission rates are R_{12} (W_{12}) and R_{21} (W_{21}), respectively. $A_{21} = 1/\tau$ describes the spontaneous transitions from the exicited state to the ground state; τ is the radiative lifetime assumed to coincide with the fluorescence lifetime.

The time behaviour populations N_1 and N_2 of the two levels can be modelled by rate equations:

$$
(1) \qquad \frac{dN_1}{dt} = -(R_{12} + W_{12})N_1 + (A_{21} + R_{21} + W_{21})N_2
$$

$$
(2) \qquad \frac{dN_2}{dt} = -\frac{dN_1}{dt}
$$

The transition rates are given in terms of the mode intensity profiles I_p and I_s and cross-sections σ_{lm} (absorption (lm=12) and emission (lm=21)); in particular, the pump/signal absorption and emission rates are proportional to the intensity profiles and can be written as:

$$
R_{lm}(x,y,z,t,\lambda_p) = \frac{\sigma_{lm}(\lambda_p)}{hc/\lambda_p}\, I_p(x,y,z,t,\lambda_p)
$$

$$
W_{lm}(x,y,z,t,\lambda_s) = \frac{\sigma_{lm}(\lambda_s)}{hc/\lambda_s}\, I_s(x,y,z,t,\lambda_s)
$$

$$
(3) \qquad lm = 12,21
$$

h is Planck's constant, c the vacuum velocity of light. In addition the both intensity profiles I_j for $j = p,s$ can be factorized:

$$
(4) \qquad I_j(x,y,z,t,\lambda_j) = P_j^0\, j(z,t)\, j_0(x,y,\lambda_j)
$$

Here, P_p^0 and P_s^0 are the launched pump and signal powers with an evolution along the propagation direction described by $p(z,t)$ and $s(z,t)$. The transversal intensity distributions (p_0, s_0) of the modes are normalized by an integration over the waveguide cross-section: $\int j_0(x,y,z,\lambda_j)\,dA = 1$ $j = p, s$. x, y are defined as transversal, vertical direction of the waveguide cross section, respectively (see Fig. 2).

The total population density $N_0(x,y)$, which corresponds to the Er-dopant concentration, can be written as $N_0 = N_1 + N_2$ and is time–independent. With $N = N_2 - N_1$ as definition of the *inversion* the following ordinary differential equation can be obtained:

$$
\begin{aligned}
\frac{dN}{dt} &= (R_{12} - R_{21} + W_{12} - W_{21} - A_{21})\,N_0 \\
&- (R_{12} + R_{21} + W_{12} + W_{21} + A_{21})\,N \\
N &= N(x,y,z,t)
\end{aligned}
$$
(5)

Light propagation and interaction. The evolution of the forward and backward propagating pump/signal intensities is based on the equation of continuity for a gain medium [8]:

$$
\left(\pm\frac{\partial}{\partial z} + \frac{1}{c_n}\frac{\partial}{\partial t} \right) I_j^\pm(z,t) = g_j\, I_j^\pm(z,t) \pm \chi_j
$$

$$
\begin{aligned}
g_j &= -\tilde{\alpha}_j + \sigma_j^{21} N_2 - \sigma_j^{12} N_1 \\
j &= p, s
\end{aligned}
$$

$(\pm c_n \partial_z + \partial_t)\, I_j^\pm(z,t) = 0$ would describe the pure light propagation of the modes' intensities with light velocity inside the substratum. Hence, the right side of our equation gives its losses (by absorbtion: σ_j^{12} and by scattering: $\tilde{\alpha}_j$) and its winnings (by spontanous emission: χ and by induced emission: σ_j^{21}). c_n is the velocity of light in the medium with (effective) refractive index n; $\tilde{\alpha}$ describes the wavelength dependent scattering losses. An integration over the waveguide cross section taking into account the normalization conditions leads to the following differential equations for the intensity amplitudes $j^\pm(z,t), j = p, s$, of the forward $(+)$ and backward $(-)$ running modes:

$$
\left(\pm\frac{\partial}{\partial z} + \frac{1}{c_n}\frac{\partial}{\partial t} \right) j^\pm(z,t) = \tilde{g}_j\, j^\pm(z,t) \pm \tilde{\chi}_j
$$
(6)

$$
\tilde{g}_j = -\tilde{\alpha}_j + \frac{1}{2}(\sigma_j^{21} - \sigma_j^{12}) \int N_0 j_0\, dA
$$
(7)

$$
+ \frac{1}{2}(\sigma_j^{21} + \sigma_j^{12}) \int N j_0\, dA
$$
(8)

$$
j = p, s
$$

This system of coupled partial differential equations has to be solved taking into account the boundary conditions at $z = 0$ and $z = l$ (see also Fig. 4):

$$
s^+(0,t) = R_1(\lambda_s)\, s^-(0,t)
$$
(9)

$$
s^-(l,t) = R_2(\lambda_s)\, s^+(l,t)
$$
(10)

$$
p^+(0,t) = R_1(\lambda_p)\, p^-(0,t) + \eta\frac{P_{p,ex}^0(t)}{P_p^0}
$$
(11)

$$
p^-(l,t) = R_2(\lambda_p)\, p^+(l,t)
$$
(12)

4

R_1, (R_2) is the reflectivity of the front (rear) mirror, respectively. $P^0_{p,ex}$ describes the incident pump power, P^0_p the power for the forward propagating wave with an evolution along the propagation direction described by $p^+(z,t)$. η is the pump coupling efficiency.
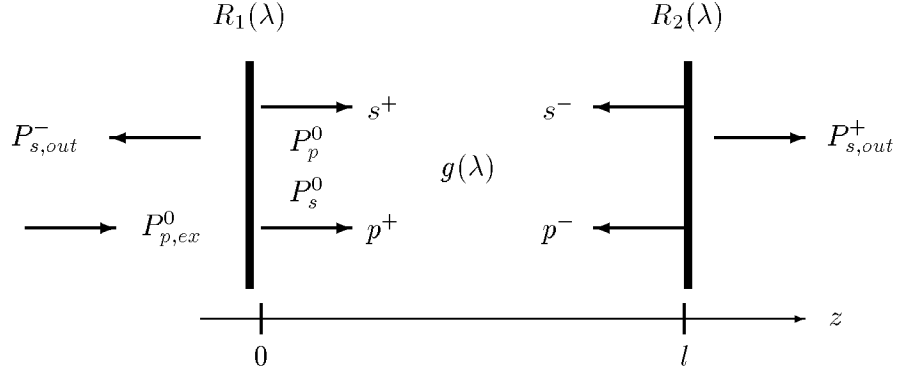

FIG. 4. *Laser-cavity with wavelength dependent reflectivities for the front (R_1) and rear (R_2) mirror. $P^0_{p,ex}$ is the incident pump power, P^0_p (P^0_s) the pump (signal) power within the cavity with an evolution along the propagation direction described by p^+ (s^+) and $P^{\pm}_{s,out}$ the forward and backward output power of the signal. $p^{\pm}$ and $s^{\pm}$ are the amplitudes of the forward and backward propagating intensities. The gain medium is described by $g(\lambda)$.*

The amplitudes of the propagating waves $p^{\pm}$ and $s^{\pm}$ vary in space and in time and can not be separated. Therefore, it is not possible to obtain an analytical solution; one has to solve the boundary value problem (BVP) numerically. Nevertheless, also the numerical solution of this coupled partial differential equation system is known to be not easy. In the next section we will see how we can replace this BVP by an initial value problem (IVP), which can be numerically handled with less effort.

3. Simplification to an Initial Value Problem. The physical model for the regarded laser system has led us to the boundary value problem (BVP) (6) with the reflection boundary conditions (9)-(12).

In this section an example-BVP

$$(13) \qquad \left(\frac{1}{c_n}\frac{\partial}{\partial t} \pm \frac{\partial}{\partial z}\right) f^{\pm}(z,t) = -g\ f^{\pm}(z,t)$$

with time-independent g and with boundary conditions

$$
\begin{aligned}
(14) && f^+(z,0) &= ae^{-gz}, & \forall z \in (0,l]\\
(15) && f^-(z,0) &= R_2\,a\,e^{g(z-2l)}, & \forall z \in [0,l]\\
(16) && f^+(0,t) &= \alpha + R_1 f^-(0,t), & \forall t > 0\\
(17) && f^-(l,t) &= R_2\,f^+(l,t), & \forall t > 0
\end{aligned}
$$

with $\alpha, a > 0$ to be discussed. The question we are interested in is: *Can this BVP be replaced by a simpler problem, whose solution takes less computational effort?*

Herein an initial value problem (IVP) is constructed, whose solution, under certain conditions, is an excellent approximation of the BVP's solution. At the end of this section it will be demonstrated how the particular form of these conditions opens the possibility to transfer this procedure (replacement of the BVP by an IVP) to our physical problem (6).

According to Lagrange the general solution of (13) is

$$(18) \qquad f^{\pm}(z,t) = \exp(\mp gz)\,\psi^{\pm}(z \mp c_n t)$$

with a free (only differentiable) function ψ, which is to determine from the boundary conditions. With (18) the boundary conditions (14)-(17) read

$$(19) \qquad \psi^{+}(x) = a, \qquad\qquad \forall x \in (0, l]$$

$$(20) \qquad \psi^{-}(x) = R_2 a\, e^{-2gl}, \qquad \forall x \in [0, l]$$

$$(21) \qquad \psi^{+}(-x) = \alpha + R_1\,\psi^{-}(x) \quad \forall x$$

$$(22) \qquad \psi^{-}(x+2l) = R_2\, e^{-2gl}\,\psi^{+}(-x)\ \forall x$$

For simplification let us introduce $\beta := R_1\,R_2\,e^{-2gl}$ and $\gamma := R_2\,e^{-2gl}$. One can compute the following interesting result: For $m \in N_0$ the $\psi^{\pm}$ are given by

$$(23) \qquad \psi^{+}(x) = \beta^{m+1}a + \sum_{n=0}^{m} \beta^n\, \alpha, \qquad -(m+1)2l < x \leq -m2l$$

$$(24) \qquad \psi^{-}(x) = \gamma\left(\beta^{m+1}a + \sum_{n=0}^{m} \beta^n\, \alpha\right), \qquad (m+1)2l \leq x < -(m+2)2l$$

This can be proved by induction on m, where the induction steps (for $m = 0$ and $m \to m+1$) result straightforward from (19)-(22).

Now we can evaluate the geometric sum in (23) and put it into (18). As the result we are getting the solution of the BVP (13) with boundary conditions (14)-(17):

$$(25) \qquad f^{+}(z,t) = e^{-gz}\left(\beta^{m+1}a + \frac{1-\beta^{m+1}}{1-\beta}\,\alpha\right), \qquad \frac{m2l+z}{c_n} \leq t < \frac{(m+1)2l+z}{c_n}$$

$$(26) \qquad f^{-}(z,t) = \gamma e^{+gz}\left(\beta^{m+1}a + \frac{1-\beta^{m+1}}{1-\beta}\,\alpha\right), \qquad \frac{(m+1)2l-z}{c_n} < t \leq \frac{(m+2)2l-z}{c_n}$$

for $z \in [0, l]$ and $m \in N_0$.

Our solutions (25), (26) are piecewise continous only. For numerical reasons this is not the finest result. But we can find continous approximations of them (see Fig. 5): If $t \gg \frac{2l}{c_n}$, the m to choose in (25), (26) is approximately given by $m + 1 = \frac{c_n t}{2l}$ so that for those t we can write

$$f^{+}(z,t) = e^{-gz}\left(\beta^{\frac{c_n}{2l}t}a + \frac{\alpha}{1-\beta}\left[1 - \beta^{\frac{c_n}{2l}t}\right]\right)$$

$$f^{-}(z,t) = \gamma\, e^{gz}\left(\beta^{\frac{c_n}{2l}t}a + \frac{\alpha}{1-\beta}\left[1 - \beta^{\frac{c_n}{2l}t}\right]\right)$$

After all this, the result $(\gamma f^{+}e^{gz} = f^{-}e^{-gz})$ justifies the form of the initial conditions (14) and (15). To compute the 'total intensity' $f := f^{+} + f^{-}$ let us define

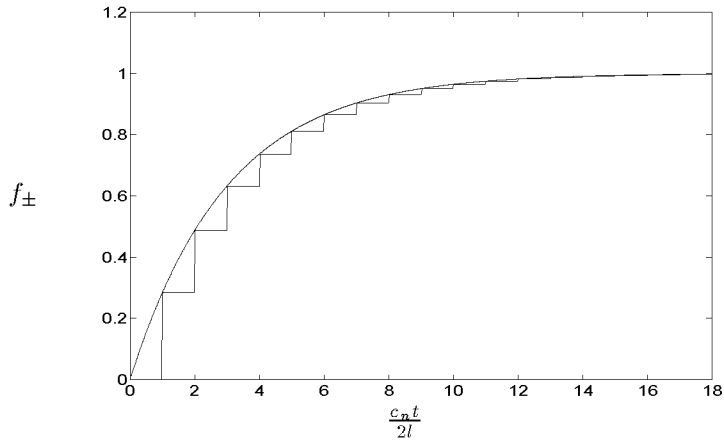$$(27) \qquad \kappa(z) := e^{-gz} + \gamma e^{gz}$$

FIG. 5. *This is the typical situation of our approximation above (with $f_\pm$ normalized to 1). The stepwise exact solution is well approximated by the continuos one for all t with $\frac{c_n t}{2l} \gg 1$.*

Now we can use $\beta^{\frac{c_n}{2l}t} = \exp\left(\frac{c_n \ln \beta}{2l}t\right)$ to get

$$
(28) \qquad f(z,t) \;=\; \left[\frac{\alpha}{1-\beta}\left(1 - \exp(\frac{c_n \ln \beta}{2l}t)\right) + a\exp(\frac{c_n \ln \beta}{2l}t)\right] \kappa(z)
$$

Hence we see that for $t \gg \frac{2l}{c_n}$ the solution of the IVP

$$
(29) \qquad \frac{1}{c_n}\frac{\partial f(z,t)}{\partial t} \;=\; \left(\frac{\ln R_1 R_2}{2l} - g\right) f(z,t)
$$
$$
-\frac{1}{2l}\frac{\ln \beta}{1-\beta}\kappa(z)\,\alpha
$$

with

$$
(30) \qquad f(z,0) = \kappa(z)\,a
$$

is a good approximation of the solution of our example-BVP. Fortunately this IVP has got the same initial values $f(z,0)$ as given in the BVP by (14) and (15).

This result shows how to replace the considered BVP by a family of IVP for all z. But if we are only interested in the *average total intensity inside the cavity*

$$
(31) \qquad \bar{f}(t) \;:=\; \frac{1}{l}\int_0^l f(z,t)\,dz
$$

and if the condition $g \ll \frac{1}{l}$ is fulfilled, then with a look at (27) we approximately find

$$
(32) \qquad \kappa(z) = 1 + R_2 + \mathcal{O}(gl)
$$

Thus with respect to our conditions $t \gg \frac{2l}{c_n}$ and $g \ll \frac{1}{l}$ we can regard the averaged solution $\bar{f} = \frac{1}{l}\int f^+ + f^- \, dz$ of our example-BVP as given by the computationally much cheaper solution of the IVP (29), (30) with (32).

Is that of any help for our model BVP (13)? There we have to solve a BVP for $p^\pm$ and $s^\pm$ (simultaneous with the IVP (5) for N) similar to our example-BVP but with time-dependent g_p

and g_s. In (5) we can average with respect to z without any problem (see (3)). Thus we only need the averaged total intensities $\bar{p}$, $\bar{s}$ if the $g_{p,s}$–variation is slow (they may not vary during a few round–trips $\tau = \frac{2l}{c_n}$). Hence if the $g_{p,s}$ are slow varying with respect to the time lenght $\tau = \frac{2l}{c_n}$ we can use our replacement-procedure *locally in time* even to solve the model BVP (13):

Let $j = p, s$ and T_j be a typical time-constant of the variation of g_j in a neighborhood of t. Besides let $j(z,t)$ be the solution of the model-BVP having the form of (30). Then we can compute $j(t + T, z) \approx j(t + T)$ by solving an IVP (29), (30), (32) if two conditions for g_j are fulfilled:

$$(33) \qquad\qquad T_j \;\gg\; \frac{2l}{c_n}$$

$$(34) \qquad\qquad g_j(t) \;\ll\; \frac{1}{l}$$

Using an integrator with stepsize control an efficient algorithm for solving (13) can be constructed:

1. Given: p(t), N(t), s(t)
2. Compute $g_{p,s}(t)$ from $N(t)$. Break if (34) is hurt.
3. Make an integration step for the IVP constructed from (29), (30), (32) for p and s.
4. Let τ be the stepsize of the integrator. Check (33) with $T_j = \tau$. If it is fulfilled take the results $p(t + \tau)$, $s(t + \tau)$ and $N(t + \tau)$ in 1.

In conclusion, we can use (locally in time) the above constructed replacement-procedure to reformulate our essential boundary value problem (6), (9)-(12) in form of the following initial value problem (equation (35)). Notice that ϕ_p embodies two terms: the spontanous emission constant χ_p and the additional constant term resulting from external pumping (see equation (29)). For $j = s$ the second term vanishes ($\alpha = 0$) and we obtain $\phi_s = \tilde{\chi}_s$.

$$
(35) \qquad
\begin{aligned}
\frac{1}{c_n}\frac{dj}{dt} &= \left[-\delta_j + \frac{1}{2}(\sigma_j^{21} - \sigma_j^{12}) \int N_0 j_0 \, dA \right. \\
&\qquad \left. + \frac{1}{2}(\sigma_j^{21} + \sigma_j^{12}) \int N j_0 \, dA \right] j + \phi_j \\
\delta_j &= \tilde{\alpha}_j - \frac{1}{2l} \ln\left[R_1(\lambda_j) R_2(\lambda_j) \right] \\
j &= j^+ + j^- \\
j &= p, s
\end{aligned}
$$

These equations couple to the transient behaviour of the inversion $N(x, y, t)$ (see equation (5); with p and s, N gets independent from z, too) via the integral-term $\int N j_0 dA$ and via the rate-coefficients R, W accourding to (3). This can be solved numerically as an ordinary differential equation (ODE) system by a discretization of the integral-term using the method of lines: The cross-section A of the cavity gets divided into cells C_i, $i = 1, \ldots, M$ where discretizations $n_i(n_i^0)$ represent $N|_{C_i}(N_0|_{C_i})$ and fulfil rate equations derived from (5) and (3):

$$
(36) \qquad
\begin{aligned}
\frac{dn_i}{dt} &= (R_{12}^i - R_{21}^i + W_{12}^i - W_{21}^i - A_{21}^i) \, n_i^0 \\
&\quad - (R_{12}^i + R_{21}^i + W_{12}^i + W_{21}^i + A_{21}^i) \, n_i
\end{aligned}
$$

Hence, our endeavour toward a theoretical model for the considered laser processes ends at an initial value problem for a rather big system of ordinary differential equations.

4. Algorithmic Considerations.

Numerical properties of the ODE. The ODE–system (35), (36) derived above has some properties that demand a very careful numerical solution. First of all, it represents a so-called *stiff* ODE, which may be roughly described as a system whose solution components locally are strongly decreasing. In other words, the linearization of the ODE has eigenvalues with small real parts. The stability theory of numerical intergration (cf. [6]) shows that for systems of this kind *implicit* discretization schemes (like implicit Runge-Kutta methods) are strongly preferable over explicit ones. Using an explicit method, the stepsize has to be chosen very small in order to reflect the asymtotic behavior of the solution. Thus, an explicit method becomes very inefficient (if there is an appropriate stepsize control) or gives a completely wrong solution. In some cases the stepsize has to be so small that roundoff errors dominate the solution and destroy any useful information.

On the other hand, implicit methods allow much bigger stepsizes without getting out of control of the ODE's stability properties (Their "stability domain" covers a large part of the left half of the complex plane). There is one major drawback concerning implicit methods: In each integration step we have to solve at least a linear system of the problem's dimension. That is, why we are going to discuss the efficient solution of the arising linear systems in our particular case below.

The second crucial property of the ODE system is its nonlinearity, which has to be taken into account for a robust and efficient stepsize control. Fortunately, implicit methods bear enough information about the linearization of the problem which can be employed to monitor the nonlinear effects and to reduce the stepsize if neccessary.

There is a third characteristic which is of much importance for the numerical simulation: By its physical meaning the intensity s is a positive value, a property, which should be maintained by the numerical method. In fact, a negative s leads to a numerical catastrophe, since the trajectories become unstable in that case. Therefore, we apply the simple transformation $s = u^2$ and reformulate the ODE in terms of the new variable u.

The results in this paper have been obtained using a new version of the semi-implicit Euler extrapolation code EULSIM [3], [7]. It is provided with an adaptive order and stepsize control [2] minimizing the numerical effort for the local subproblems. Due to the automatically chosen variable orders of the extrapolation method, we do not need any a priori information about which order fits the problem. In addition, the code incorporates a device that keeps track of the nonlinearity of the problem. This nonlinearity monitor increases the robustness of the code drastically and allows much weaker accuracy demands without loosing qualitative information about the solution.

Solution of the linear systems. For the semi-implicit Euler discretization we have to solve linear systems

$$Jx = b, \quad J = I - hA,$$

where A is the Jacobian of the ODE's right hand side and h the stepsize of the semi-implicit Euler step. In the present situation, the Jacobian A has the very simple structure of a diagonal

9

matrix with two additional non-vanishing colums and rows:

$$A = \begin{bmatrix} * & & & & * & * \\ & \ddots & & & \vdots & \vdots \\ & & & * & * & * \\ * & \cdots & * & * & * & 0 \\ * & \cdots & * & * & 0 & * \end{bmatrix}$$

Obviously the transition to the matrix $J = I - hA$ does not alter this structure, so that we are left with matrices

$$J = \begin{bmatrix} d_1 & & & & v_1^s & v_1^p \\ & \ddots & & & \vdots & \vdots \\ & & & d_m & v_m^s & v_m^p \\ u_1^s & \cdots & u_m^s & d_{n-1} & 0 \\ u_1^p & \cdots & u_m^p & 0 & d_n \end{bmatrix}$$

where $m = n - 2$. Moreover, we may assume that $d_i \neq 0$ for all $1 \leq i \leq n$ and h small enough. In this case it is easy to give an explicit LR decomposition $LJ = R$ of J by

$$L = \begin{bmatrix} 1 & & & & \\ & \ddots & & & \\ & & 1 & & \\ \tau_1^s & \cdots & \tau_m^s & 1 & \\ \bar{\tau}_1^p & \cdots & \bar{\tau}_m^p & -\delta/\alpha & 1 \end{bmatrix} \qquad R = \begin{bmatrix} d_1 & & & v_1^s & v_1^p \\ & \ddots & & \vdots & \vdots \\ & & d_m & v_m^s & v_m^p \\ & & & \alpha & \gamma \\ & & & & \beta - \delta\gamma/\alpha \end{bmatrix}$$

where $\tau_i^s = -u_i^s/d_i$, $\bar{\tau}_i^p = \tau_i^p - \frac{\delta}{\alpha}\tau_i^s$, $\tau_i^p = -u_i^p/d_i$ and

$$\alpha = d_{n-1} + \sum_{i=1}^m v_i^s \tau_i^s, \quad \beta = d_n + \sum_{i=1}^m v_i^p \sigma_i^p, \quad \gamma = \sum_{i=1}^m v_i^p \tau_i^s, \quad \delta = \sum_{i=1}^m v_i^s \sigma_i^p .$$

Since we abandoned any pivoting, the solution of $Jx = b$ via the LR-decomposition derived above may be instable. Therefore we use iterative refinement until the componentwise backward error

$$\eta = \max_{1 \leq i \leq n} \frac{|Jx - b|_i}{(|J| |x| + |b|)_i}$$

satisfies $\eta < \sqrt{\epsilon}$, where ϵ denotes the relative machine precision. In our experience at most two iterative refinement steps were sufficient.

The semiimplicit Euler discretization requires three subroutines (besides the evaluation of the right hand side):

    a) evaluation of the Jacobian A

    b) computation and decomposition of $J = I - hA$

    c) solution of the linear system $Jx = b$ (for different b)

For a) we have to compute and store the non-vanishing entries of A. In the second step b), we directly calculate the elements τ_i^s, τ_i^p, α, β, γ and δ requiring $\sim 12\,n$ flops. For each right hand side b the computation of $x = R^{-1}Lb$ needs $\sim 12(k+1)\,n$ flops, where k is the number for iterative refinement steps. It is worth pointing out that we need a storage of only $10\,n$ real numbers to save A together with the LR-decomposition of J. If n is about 400 (so it is in our simulation calculations presented in the next sections) this is a considerable reduction of storage effort.

10

5. Simulation results. In this section the numerically calculated results of relaxation oscillations in a planar Er-diffused Ti:LiNbO$_3$ dielectric waveguide laser are presented and discussed. As in many problems our model equations contain several unknown parameters. For example, the Er-dopant distribution N_0, which must be determined from a model describing the specific indiffusion process of the Er^{3+}–ions, the intensity distribution $i_0(x, y, \lambda)$, which depends on the geometric properties of the waveguide, or the wavelength–dependent cross sections $\sigma(\lambda)$, which can be calculated by analysing the absorption and emission spectra of the given material. In order to describe one particular experiment (relaxation oscillations in an Er-diffused Ti:LiNbO$_3$ waveguide laser) one has to determine each of these parameters according to this specific situation. We have done this in each case according to the considerations made in [4]. The technical data of the herein considered laser are precisely listed up in [4]; a detailed description of its realization is given in [1].

The results have been obtained by numerically integrating the equations (35) and (36) (see section 2). Both, the time dependent pump- and signal intensity evolution are analyzed. Moreover, the population densities of the ground ($N_1(x, y, t)$) and the excited state ($N_2(x, y, t)$) and the inversion ($N = N_2 - N_1$) as functions of time and space will be discussed. In all following figures the physical quantities (p, s, N_i) are given in *normalized units* [nu]. All over this report they are the same, hence all figures allow direct comparisons. If you want to compute the real intensities from these data you have to use the following equations:

- If s is given in [nu], the signal output power in forward direction behind the rear mirror is given by $P^+_{s,out} = \frac{(1-R_2)P^0_s}{1+R_2} s$ with $R_2 = 0.95$ and $P^0_s = 40 \, \text{mW}$, while the total signal intensity inside the cavity is $P_{s,in} = s \, P^0_s$.
- The normalized input power p_{in} and the external incident power $P^0_{p,ex}$ are connected by $P^0_{p,ex} = p_{in} \cdot 80 \, \text{mW}$.
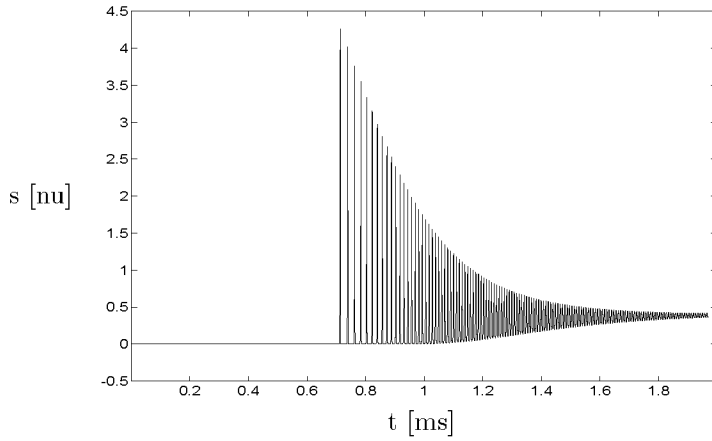

FIG. 6. *Calculated relaxation oscillations of an erbium-diffused Ti:LiNbO$_3$ waveguide laser: signal output power ($\lambda_s = 1.574 \, \mu m$) in forward direction versus time*

We consider a step-function pump rate for the coupled pump power, which means that $p_{in}(t) = 0$ for $t < 0$ and $p_{in}(t) = 1$ for $t > 0$. The initial conditions for the calculation are $N(x_i, y_j, t) = -N_0(x_i, y_j), i = 1..16, j = 1..25$ (remember N_0 is the (local doped) Er-concentration profile), $s(t = 0) = \tilde{\chi}_s$ (s_0 represents the spontaneous emission necessary to start the laser action) and $p(t = 0) = 1$.

As a representative example, Fig. 6 presents the calculated signal output power as a function of time. At the beginning the amplitude of the signal power is very low. At a specific time
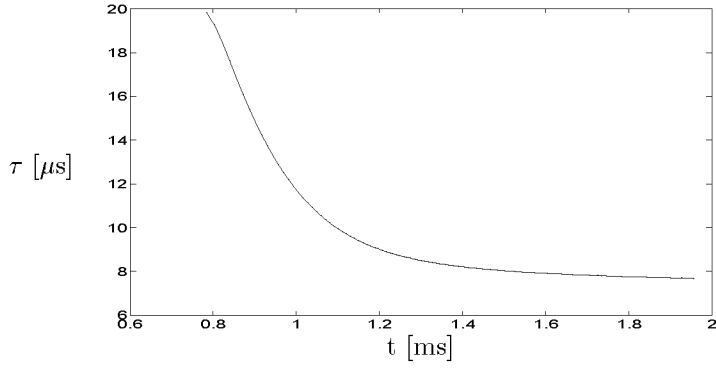
11

FIG. 7. *Calculated time-dependent repetition period (τ) versus time.*

$t_{osc} = 0.61$ ms the behaviour changes tremendously: a sequence of fairly sharp pulses set in with a time dependent repetition rate $\tau(t)$, whose monotonous decrease is shown explicitely in Fig. 7. The envelope of these pulses follow a damped exponential like function with a characteristic damping rate as it has almost been demonstrated for different laser systems. After about 2 ms s reaches the steady state of constant output power. This behaviour is called *relaxation oscillation*.

5.1. Comparison with experiments. Exactly the same laser we have computed our model's input parameters for was used to measure its signal output data versus time. The result is shown in Fig. 8.
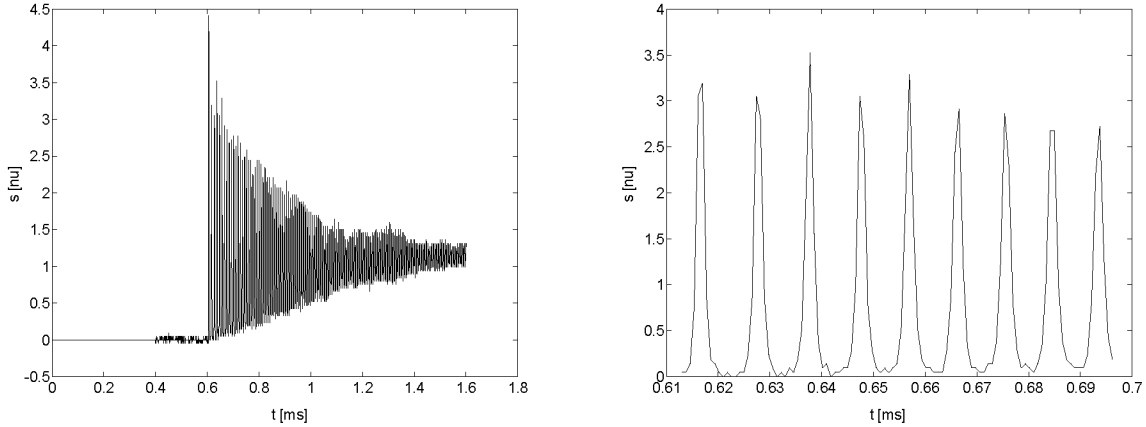
FIG. 8. *Measured relaxation oscillations of an erbium-diffused Ti:LiNbO₃ waveguide laser: signal output power ($\lambda_s = 1.574\,\mu m$) in forward direction versus time (left) and enlargement of some peaks (right).*

The direct comparison of the results from calculation and experiment in Fig. 9 shows that the characteristics of the calculated data meets those of the measured ones (qualitatively and nearly quantitatively): exponential damping, onset time, sharpness of the pulses and (as a look to the enlargement in Fig. 8 shows) time dependent repetition rate.

Little deviations need not necessarily be seen as inaccurasies of the theoretical model: even the indirect determination of the input parameters and the measurement of the signal output are complex investigations; therefore they are a source of error themselves.
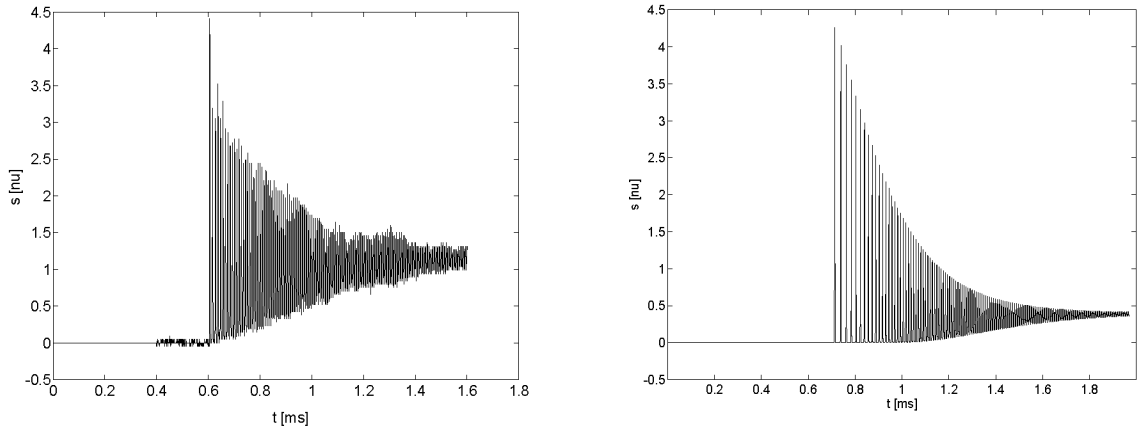
FIG. 9. *Measured (left) and calculated (right) relaxation oscillations of an erbium-diffused Ti:LiNbO₃ waveguide laser: signal output power ($\lambda_s = 1.574\,\mu m$) in forward direction versus time .*

5.2. Data available from simulation. In the following we present a lot of other data which results form the presented simulation calculation. For these data no experimental comparison can be made, because they are either simply non–measurable (as the occupation densities) or not measured till today. Therefore the following paragraph will draw a rough picture of the physical mechanism lying beyond the process of relaxation oscillations. After this we will look at the named data trying to interpret them in the given way.
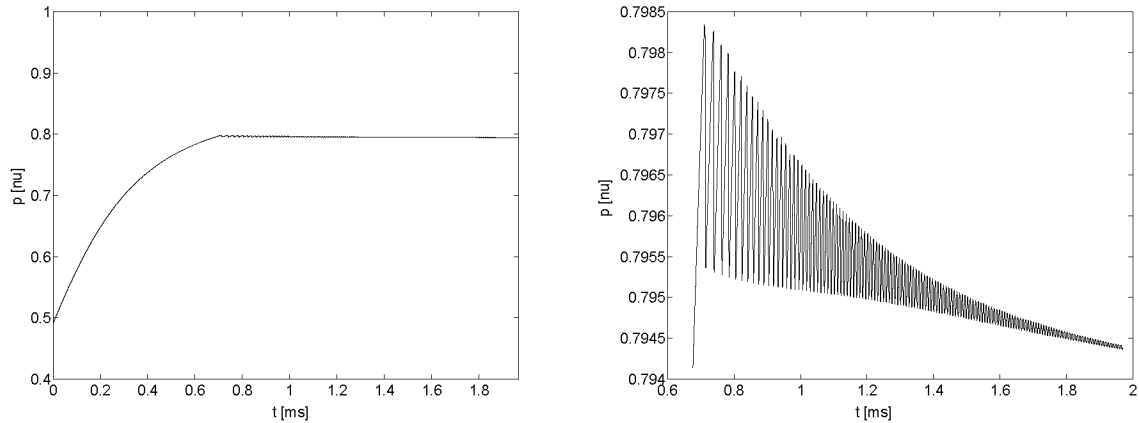

FIG. 10. *Calculated evolution of the coupled pump power ($\lambda_p = 1.478\,\mu m$) as function of time of an erbium-diffused Ti:LiNbO₃ waveguide laser (left) and an enlarged part of its quasiconstant state (right).*

In general the process of relaxation oscillations can be interpreted physically as an interplay between signal s, pump p, and the population densities (N_1 and N_2). At the beginning, where the amplitude of the signal is very low, energy from the pump is used to build up the inversion $N_2 - N_1$: the population of the ground state decreases and the excited state, corresponding to the laser level, increases. Whereas this time, the value of the pump amplitude is less than the incident amplitude (due to absorption) and increases exponentially against a position of equilibrium (saturable absorber). At t_{osc} the inversion has become big enough to slowly increase s due to emission. The buildup of s from its initial value produced by spontaneous emission takes some time; whereas this time the inversion can continue to grow until the signal amplitude overcomes

13

a specific value. Than $N(t)$ decreases due to the increased rate of stimulated transitions. After its maximum the signal starts to decrease but as long as it is big enough it further decreases the inversion. As a result the inversion is small enough to again be build up by the pumping process and so on.

In contradiction to previous descriptions also the transient behaviour of the pump p has to be considered. In time regions with low s — in particular between two neighboring pulses — p (respectively N) increases exponentially. During the single pulses the pump amplitude decreases because more pump energy is needed to again build up the decreasing inversion. It is worth to notice that the described process depends on the overlap of the pump, the signal and the locally defined inversion: it is obvious that inversion can only be reached in space regions with sufficient pump intensity, i.e. in the center of each cross section of the waveguide.

As a representative example, Fig. 10 present the evolution of normalized pump output power versus time. After the exponential increase ($t < t_{osc}$) the output seems to be slightly constant. However, enlarging this part from the pump evolution (Fig. 10 (right)) the oscillatory behaviour of the pump is obvious, but small. The above explained relationship between pulses in s and regions of increase and decrease in p and N can be seen in detail in Fig. 11. Notice the magnification of $p(N)$ in Fig. 11; for this diagram N represents the time dependent inversion in one specifically chosen point (x_i, y_j) lying next to the maximum of the signal intensity distribution.
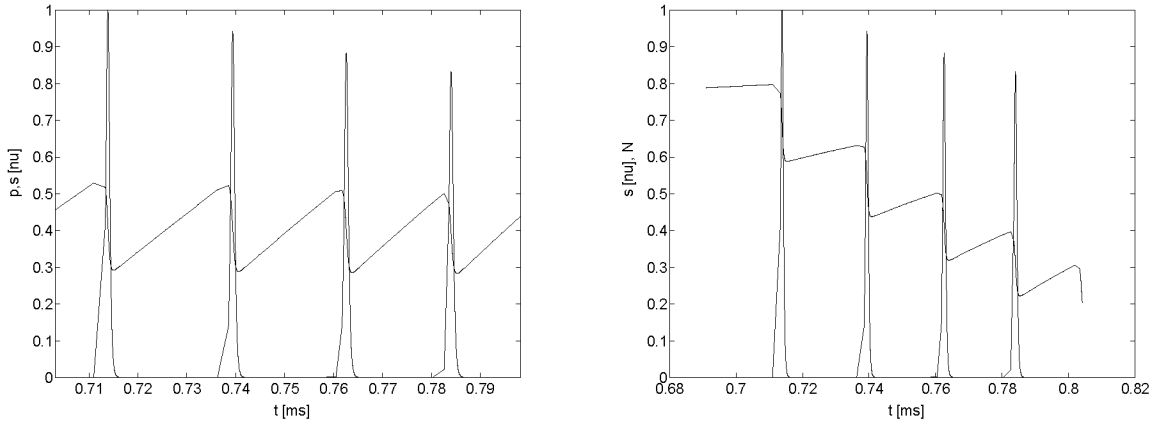

FIG. 11. *Calculated evolution of the coupled pump power (p) and the signal output power in forward direction (s) (left) and of the inversion of one discrete point in the waveguide cross section and the signal output (s) (right). Both versus time. Enlarged parts of Fig. and Fig. . Mark the simultanous variations in three observables.*

According to Fig. 2 a vertical (y) and a lateral (x) cut through the waveguide cross section have been chosen to demonstrate the *space* dependency of the inversion. The 3d–graphic in Fig. 12 shows the normalized distribution $\hat{N}_1(x, t) := N_1(x, y_j, t)/N_0(x, y_j, 0)$. Due to the waveguide symmetry only the right part ($x > 0$) is plotted. In the periphery ($x > 8\,\mu$m) the transient behaviour of the ground state is slightly constant, whereas in the center of the cross section (maximum of $p_0(x, y)$!) the exponential decay of N_1 and the beginning of the stepwise behaviour can be seen.

Fig. 13 shows the stepwise part in more detail. It demonstrates that the single steps of N_1 appear *simultanously* in the whole cut.
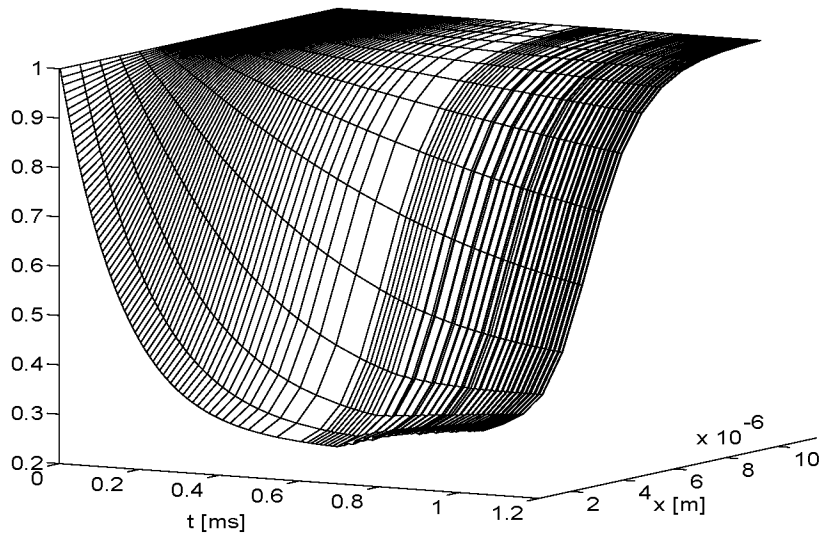
FIG. 12. *3D-graphic of a lateral cut (x in µm) through the waveguide's cross section versus time (in ms). The distribution has been normalized according to $\hat{N}_1(x,t) := N_1(x, y_i, t)/N_0(x, y_i, 0)$. Due to the waveguide symmetry only the part $x > 0$ is plotted. The exponential decay of the population N_1 of the ground state in the active center of the waveguide (near $x \approx 0$) can clearly be seen.*
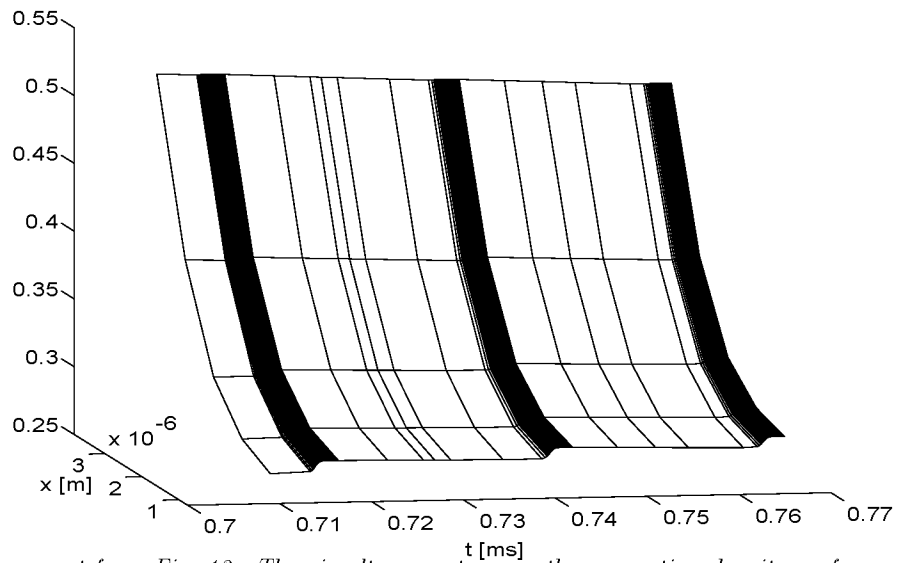

FIG. 13. *Enlargement from Fig. 12. The simultanous steps on the occupation density surface are synchron to peaks in the output signal s.*

5.3. Predictions. Naturally it is of highest interest to answer the question of how to influence the relaxation oscillations of a given waveguide laser. There are several external parameters which allow big influences on the dynamical behaviour of the laser: the external pump input (variation of its value and of its form as a function of time), the mirror reflectivities (varying the rear reflectivity ; "Q–switched laser") ...

In this section on one hand we want to demonstrate the possibilities of the presented simulation method. On the other hand we want to simulate taking influence on the dynamical behaviour of the considered laser from section 5. Therefore we ask: How will relaxation oscillations change if we remove the time independence of the external pumping?
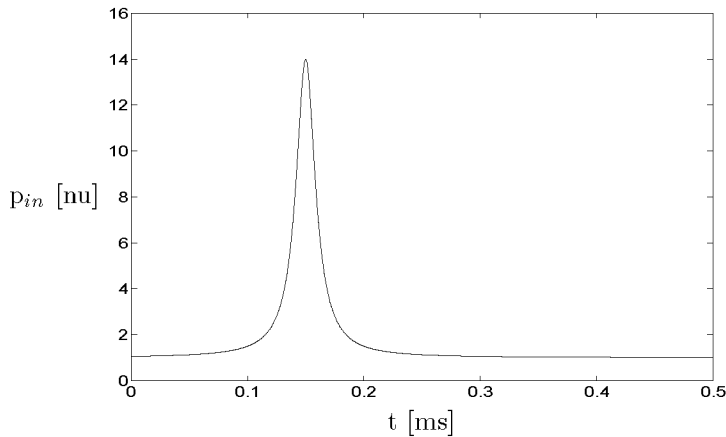

FIG. 14. *First 0.5 ms of the peaked normalized pump input power. For $t > 0.5$ ms the normalized pump input power is furthermore about 1.*

In particular we have chose exactly the same laser parameters as those in section 5. Only the time independence of the external pump has been removed: we have added a peak of about $40\,\mu s$ width at $t = 0.15$ ms after the onswitch of the pump at $t = 0$. Hence the external pump gets the form shown in Fig. 14: for $0 \leq t \leq 0.1$ ms and $t \geq 0.2$ ms it is about the same as that in section 5 (and therefore nearly time–independent in this region).
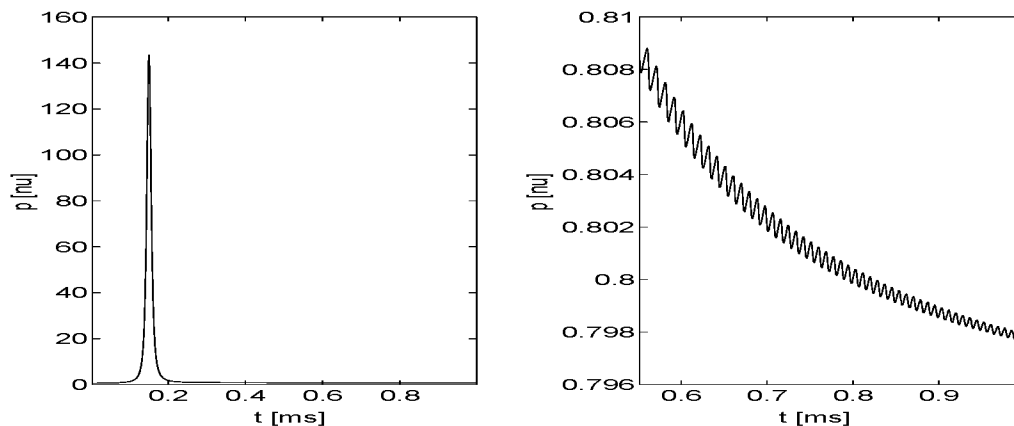

FIG. 15. *Calculated evolution of the pump power p inside the cavity for an erbium-diffused $Ti:LiNbO_3$ waveguide laser with peaked external pump and enlargement.*

According to the calculations the response of the laser to this external peak is that shown in the following figures. They must be regarded in comparison to the results presented in section 5.

16

Fig. 15 shows the computed reaction of the pump–intensity p inside the cavity. The external peak leads to an simultanous, very intense peak inside the cavity: the power of the external radiation gets accumulated inside because the losses (from absorption and at the mirrors) are less than the input. After this internal peak the relaxation oscillations of the output signal s start; as shown in Fig. 16. The single pulses in s are simultanously attended by puls–like variations in p (which are shown in the enlargement in Fig. 15 and by steps in the occupation density N_1 (see Fig. 17).
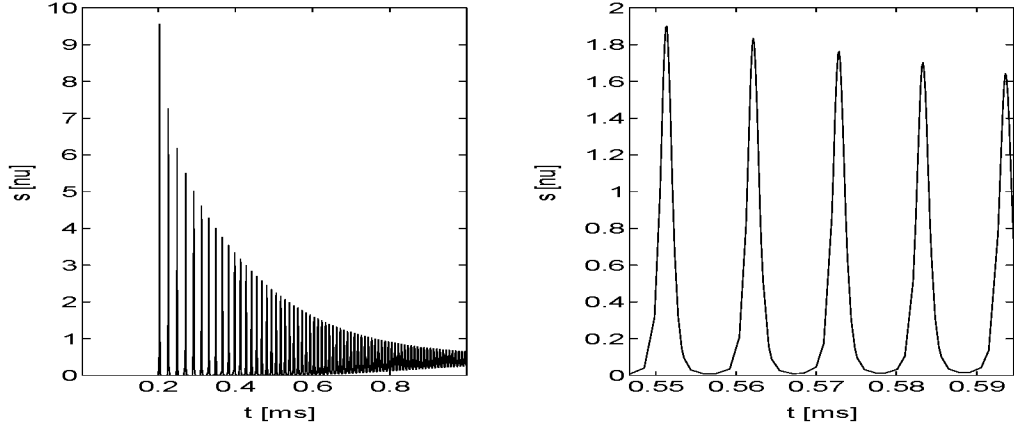

FIG. 16. *Calculated relaxation oscillations of the signal intensity s inside the cavity for an erbium-diffused Ti:LiNbO₃ waveguide laser with peaked external pump and enlargement.*

The reason for the earlier onset of the relaxation oscillations (compared with those presented in the last section) can be seen in the acceleration of the decay of the ground state occupation N_1 caused by the intense p–pulse (compare Fig. 17 and Fig. 12).

To our knowledge this scenario has never been investigated till today. Hence this section can be understood as a prediction depending on our new simulation technique.

6. Conclusions. A theoretical model for an analysis of relaxation oscillations in local Er-doped optically pumped waveguide lasers has been presented. The basic parameters of the oscillations, such as the onset, the time-dependent repetition period, the decay time and the pump- and signal output power have been able to be numerically calculated as a function of different laser input parameters, like the local Er-concentration, the intensity profiles, the scattering losses, the endface reflectivities and the cavity lengths. First results for an Er-diffused Ti:LiNbO₃ waveguide laser have been presented with a nearly quantitative agreement of theory and experiment.

The presented simulation technique makes non–measurable data (as the space- and time-dependent population density of the dopant ions) accessible. Therefore it facilitates the understanding of the laser properties of different laser types. As a cheap tool it can help to develop optimized laser structures.
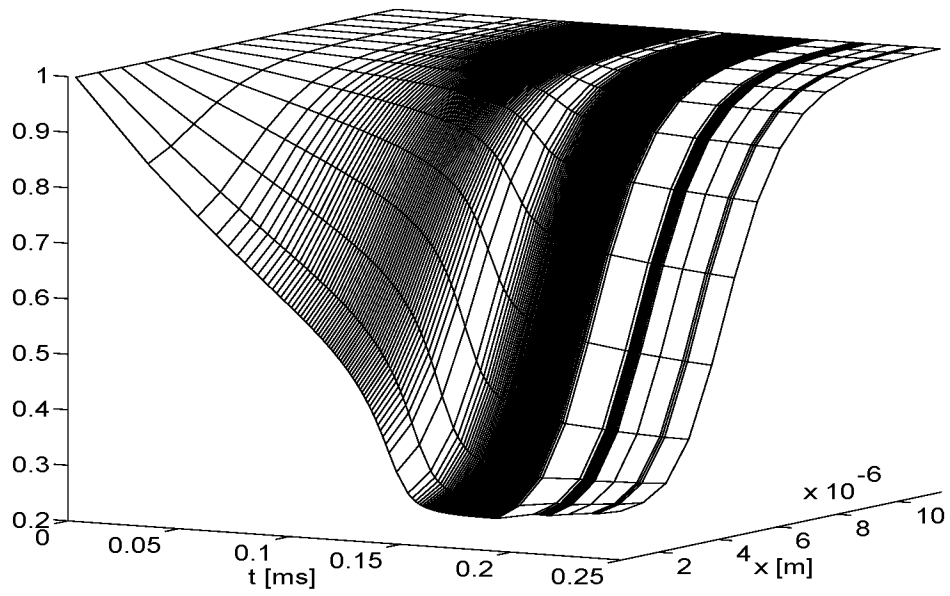
FIG. 17. *Population dynamic of $\hat{N}_1(x,t)$: a lateral cut (x in μm) through the waveguide's cross section versus time (in ms). Compare Fig. 12.*

REFERENCES

[1] P. BECKER, R. BRINKMANN, M. DINAND, W. SOHLER, AND H. SUCHE, *Erbium – diffused* LiNbO$_3$ *waveguide – laser of 1563 and 1576 nm emission wavelength*, Appl. Phys. Lett., (1992), p. 1257.

[2] P. DEUFLHARD, *Order and stepsize control in extrapolation methods*, Numer. Math., 41 (1983), pp. 399–422.

[3] ———, *Recent progress in extrapolation methods for ordinary differential equations*, SIAM Rev., 27 (1985), pp. 505–535.

[4] M. DINAND AND C. SCHÜTTE, *Theoretical modelling of relaxation oscillations in er-doped waveguide-lasers*, submitted to J. Lightw. Tech., (1993).

[5] M. DINAND AND W. SOHLER, *Theoretical modelling of optical amplification in er-doped ti:linbo3-waveguides*, submitted to J. Lightw. Tech., (1993).

[6] E. HAIRER AND G. WANNER, *Solving Ordinary Differential Equations II, Stiff and Differential-Algebraic Problems*, Springer Verlag, Berlin, Heidelberg, New York, Tokyo, 1991.

[7] A. HOHMANN, *An implementation of extrapolation codes in C++*, Technical Report TR 93–8, Konrad-Zuse-Zentrum, Berlin, 1993.

[8] P. W. MILONNI AND J. H. EBERLY, *Laser*, John Wiley and Sons, Chap. 10, 1988.